Numerical modelling of punching shear failure of RC flat slabs with shear reinforcement

Andri Setiawan

Former PhD Student, Department of Civil and Environmental Engineering, Imperial College London, London, United Kingdom

Robert L Vollum

Reader in Concrete Structures, Department of Civil and Environmental Engineering, Imperial College London, London, United Kingdom

Lorenzo Macorini

Reader in Structural Engineering, Department of Civil and Environmental Engineering, Imperial College London, London, United Kingdom

Bassam A Izzuddin

Professor of Computational Structural Mechanics, Department of Civil and Environmental Engineering, Imperial College London, London, United Kingdom

Corresponding author: Robert L Vollum (r.vollum@imperial.ac.uk)

AUTHOR'S VERSION

Abstract

This paper utilises nonlinear finite element analysis with 3-D solid elements to gain insight into the role of shear reinforcement in increasing punching shear resistance at internal columns of flat slabs. The solid element analysis correctly captures the experimentally observed gradual decrease in concrete contribution to shear resistance with increasing slab rotation and failure mode but is very computationally demanding. As an alternative, the paper presents a novel approach in which 3-D joint elements are combined with nonlinear shell elements. Punching failure is modelled with joint elements positioned around a control perimeter located at 0.5d from the column face (where d is the slab effective depth). The joint elements connect the nodes of shell elements located to either side of the punching control perimeter. The punching resistance of the joints is related to the slab rotation using the failure criterion of the Critical Shear Crack Theory. The joint-shell punching model (JSPM) considers punching failure both within the shear-reinforced region and due to crushing of concrete struts near the support region. The JSPM is shown to accurately predict punching resistance whilst requiring significantly less computation time than 3-D solid element modelling.

Notation

A_s	cross-sectional area of single shear reinforcement (e.g. stud)
A_{st1}, A_{st2}	total areas of shear reinforcement (smeared) in the 1st and 2nd perimeters respectively
A_{si}	cross-sectional area of shear reinforcement bar *i* intersecting the critical shear crack
$A_{s-total}$	total effective area (smeared) of shear reinforcement within control perimeter b_0
E_s	Young's modulus of the shear reinforcement bars
P_u	predicted punching load (peak)
S_{act}	degree of the activation of shear studs for each individual shear reinforcement perimeter
$V_{R,crush}$	shear resistance governing the failure due to crushing of concrete struts
$V_{R,in}$	shear resistance governing the failure within the shear-reinforced region
$V_{R,out}$	shear resistance governing the failure outside the shear-reinforced region
V_R	shear resistance
V_c	concrete shear resistance
V_{cap}	governing joint punching capacity taken as the minimum of the two considered failure modes ($V_{R,in}$; $V_{R,crush}$)
V_{ext}	total vertical load applied to the slab
V_i	joint shear force at current step i
V_{i-1}	joint shear force at previous step $i-1$
V_n	nominal shear resistance against punching
V_{pp}	post-punching capacity
V_s	shear resistance provided by the shear reinforcement
$V_{w,1\ bot}$	contribution of headed studs in the 1st perimeter measured based on the strain at the bottom end of the stud
$V_{w,2\ top}$	contribution of headed studs in the 2nd perimeter measured based on the strain at the top end of the stud
$b_{0,out}$	length of the effective control perimeter measured at $0.5d$ from the position of the outermost shear reinforcement perimeter
b_0	length of the control perimeter (rounded corner) at $0.5d$ distance from the support face
d_g	maximum aggregate size (used)
d_{g0}	reference aggregate size equal to 16 mm
d_v	reduced effective depth which accounts for pullout of shear reinforcement
d_w	diameter of the shear reinforcement bars
f_{sjimax}	maximum stress at current load step in shear stud *i* of perimeter j extracted from ATENA
f_c'	specified concrete compressive strength
f_{yw}	yield strength of the shear reinforcement bars

k_{deg}	linear descending joint stiffness at Stage 3
k_i	tangent stiffness at current step i
k_{inc}	linear elastic joint stiffness at Stage 1
l_w	length of shear reinforcement bars
n_r	number of radii of shear reinforcement
n_{r1}, n_{r2}	number of stirrups (radii) in the 1st and 2nd perimeters respectively
s_0	distance between the first row of shear reinforcement and the column face
s_1	distance between two adjacent reinforcements at the same radius
β_i	angle between shear reinforcement bar *i* and the slab plane
ρ_t	shear reinforcement ratio calculated at a perimeter at $0.5d$ of the edge of the support region
ρ_w	smeared shear reinforcement ratio considering the influence of initial and consecutive shear reinforcement spacing
σ_{wi}	stress in shear reinforcement bar *i* crossing the critical shear crack calculated as a function of crack opening w_i
τ_b	bond strength
ψ_{i-1}	monitored slab rotation acquired from previous step $i-1$
L	slab span between column centrelines
d	average slab flexural effective depth
n	number of joint elements positioned along the control perimeter
w	crack width opening of the critical shear crack
w_i	crack width at shear reinforcement bar *i*
Δd_i	increment of relative joint displacement at current step i
α	constant reduction factor to reduce V_c
λ	multiplier (constant) relating the failure due to crushing of concrete struts $V_{R,crush}$ to V_c
ψ	slab rotation due to bending deformation

Introduction

The thickness of flat slabs is typically governed by considerations of deflection (Vollum, 2002; Vollum, 2009) or punching shear. Punching resistance can be enhanced through the introduction of drop panels, column heads or shear reinforcement. Of these, shear reinforcement is usually the most practical and economic. As well as increasing punching resistance, shear reinforcement increases the deformation capacity of flat slabs. This can prevent progressive collapse by enabling load redistribution between columns following localised punching (Lips, 2012). Shear reinforcement also reduces the so-called "size effect" whereby the shear stress at punching failure reduces with increasing slab depth (Birkle and Dilger, 2008; Rizk et al., 2011).

Design provisions for punching shear reinforcement can be categorised as either empirical- or mechanically-based of which ACI 318-14 (ACI, 2014) and EN 1992 (BSI, 2004) are typical of the former. By contrast, the punching provisions in Model Code 2010 (MC2010) (fib, 2013) are based on the so-called the Critical Shear Crack Theory (CSCT) of Muttoni (2008) which is a mechanically-based model. According to MC2010, punching resistance ($V_{R(w)}$) can be expressed in generalised form as:

1. $V_{R(w)} = V_{c(w)} + V_{s(w)}$

where $V_{c(w)}$ and $V_{s(w)}$ represent the concrete and shear reinforcement contributions to shear resistance respectively. The subscript w depicts the width of the critical shear crack which is assumed to be proportional to $\psi.d$ where ψ is the slab rotation due to bending deformation and d is the slab flexural effective depth. The concrete contribution ($V_{c(w)}$) reduces with increasing rotation due to increased crack width whilst the shear reinforcement contribution ($V_{s(w)}$) simultaneously increases. The effectiveness of shear reinforcement depends on its anchorage and layout as described by Lips et al. (2012) who compared the performance of double headed studs and continuous stirrups. Of these, double headed studs are most efficient due to their improved anchorage (Beutel and Hegger, 2002).

This paper extends the authors' previous numerical modelling of punching shear failure in slabs without shear reinforcement (Setiawan et al., 2019a,b, 2020) to slabs with shear reinforcement. Nonlinear finite

element analysis (NLFEA) using both 3-D solid elements in ATENA (Cervenka et al., 2018) and shell elements in ADAPTIC (Izzuddin, 1991) are considered. In each case, the NLFEA is validated using carefully selected laboratory tests. Validation of 3-D solid element modelling is in terms of load rotation and punching resistance at the global level as well as crack patterns and strain at the local level. Detailed assessment is made of the relative contributions of concrete and shear reinforcement to shear resistance as well as the percentage activation of each shear reinforcement perimeter.

Research Significance

Using 3D solid finite elements (e.g. ATENA) can produce realistic predictions of behaviour but is overly computationally intensive for other than sub-assemblies of practical structures. As an alternative, a Joint-Shell Punching Model (JSPM) is proposed. The model is an extension of that previously proposed by the authors (Setiawan et al. 2019b, 2020) for slabs without shear reinforcement. Punching failure is modelled with joint elements incorporating the failure criterion of the CSCT. The extended JSPM is validated against 12 specimens from the literature with shear reinforcement comprising eight isolated slabs and four continuous ones. The key novelty of the model, over previous implementations of the CSCT is that the failure load is calculated internally within the NLFEA without the need for post processing.

Critical shear crack theory (CSCT) and its application for slabs with shear reinforcement

Background

The CSCT (Muttoni, 2008) assumes that punching resistance is reduced by the presence of a critical shear crack which propagates through the slab into the inclined compression strut transferring load from the slab to the support. According to Muttoni and Schwartz (1991), the width of the critical shear crack is proportional to the product of slab rotation and slab effective depth ($\psi . d$). The shear force that can be transferred through the crack is assumed to depend on the crack roughness and, hence the aggregate

size. According to Muttoni (2008), the punching shear resistance (V_R) of a slab without shear reinforcement can be expressed as:

2. $$\frac{V_R}{b_0 d\sqrt{f_c'}} = \frac{0.75}{1+15\frac{\psi.d}{d_{g0}+d_g}}$$

where b_0 is the length of the control perimeter taken at $0.5d$ from the column face with rounded corners, f_c' is the specified concrete compressive strength, d_{g0} is the reference aggregate size equal to 16 mm and d_g is the maximum aggregate size used.

Fernandez Ruiz and Muttoni (2009) extended the CSCT model to include the contribution of shear reinforcement. According to Fernandez Ruiz and Muttoni (2009), three possible failure modes exist: 1) failure within the shear-reinforced region, 2) failure due to the crushing of concrete strut and 3) failure outside the shear-reinforced region (see **Fig. 1**). The governing failure mode is that giving the least resistance. This paper focusses on the first and the second failure modes (**Fig. 1(a)** and **(b)**) which are critical provided sufficient perimeters of shear reinforcement are provided. A brief description of the treatment of each failure mode in the CSCT is provided below.

Failure within the shear-reinforced region

Within the shear reinforced region, the punching resistance is calculated as (Fernandez Ruiz and Muttoni, 2009):

3. $$V_{R,in} = V_c + V_s$$

where V_c is the concrete contribution and V_s is the contribution of shear reinforcement which is expressed as:

4. $$V_s = \sum_{i=1}^{n} \sigma_{wi}(\psi).A_{si}.\sin(\beta_i)$$

where A_{si} is the cross-sectional area of shear reinforcement bar *i* intersecting the critical shear crack, β_i is the angle between shear reinforcement bar *i* and the slab plane (90° for typical vertical bars), σ_{wi} is the tensile stress in shear reinforcement bar *i* calculated in terms of the crack opening and *n* is the total number of bars of shear reinforcement crossing the critical shear crack (Fernandez Ruiz and Muttoni, 2009).

As noted by Lips (2012), **Eq. 4** is overly sensitive to the exact position of the shear reinforcement. To mitigate this, the smeared representation of shear reinforcement proposed by Lips (2012) is used in this study. Using this approach, the effective cross-sectional area (smeared) of shear reinforcement contributing to shear resistance, which is equivalent to $\sum_{i=1}^{n} A_{si}$ in **Eq. 4**, is defined as:

5. $A_{s-total} = b_0 d\rho = n_r . \frac{d_w^2}{4} . \pi \left(\frac{d}{s_0 + \frac{s_1}{2}} \right)$

where ρ is the shear reinforcement ratio, n_r is the number of radii of shear reinforcement, d_w is the shear reinforcement diameter, s_0 is the distance between the first row of shear reinforcement and the support face and s_1 is the radial distance between adjacent shear reinforcements. In this approach, the shear reinforcement stress is calculated in terms of the crack width at $0.5d$ from the support face. The stress in deformed shear reinforcement is related to the limiting crack width at which the shear reinforcement is solely activated by bond which is calculated as follows:

6. $w_{lim} = 4 . \frac{\tau_b}{E_s . d_w} . \left(\frac{l_w}{2} \right)^2$

where τ_b is the bond strength, E_s is the Young's modulus of the shear reinforcement, d_w is the shear reinforcement diameter and l_w is the shear reinforcement length.

In the smeared approach of Lips (2012), the shear reinforcement stress (σ_w) is calculated as follows:

7. $w \leq w_{lim}: \sigma_w = \sqrt{\frac{4 . \tau_b . E_s . w}{d_w}} \leq f_{yw}$
8. $w > w_{lim:} \sigma_w = \frac{E_s . w}{l_w} + \frac{2\tau_b}{d_w} . \frac{l_w}{2} \leq f_{yw}$

where f_{yw} is the yield strength of the shear reinforcement, $w = 0.25 \psi d cos\left(\frac{\pi}{4}\right)$ is the crack width at *d/2* from the column face and $\tau_b = 0.6 f_c^{2/3}$ is the bond stress.

Failure due to crushing of concrete struts near support region

The maximum possible shear resistance is limited by the compressive strength of the diagonal struts through which load is transferred into the support. This is strongly affected by their state of transverse tensile strain which depends on the slab rotation which controls the critical shear crack width. Fernandez Ruiz and Muttoni (2009) calculate the maximum possible shear resistance as a multiple, λ, of the concrete contribution alone. The magnitude of λ is dictated by the detailing of the shear reinforcement and its anchorage conditions. According to Fernandez Ruiz and Muttoni (2009), λ equals 3.0 for well-

anchored shear reinforcement (like headed studs) but should otherwise be limited to 2.0. Thus, the maximum possible shear resistance, which is limited by strut crushing, is expressed as:

9. $$V_{R,crush} = \lambda \,.\, V_c = \lambda \,.\, \frac{0.75\, b_0 \,.d\,.\sqrt{f_c'}}{1+15\frac{\psi.d}{d_{g0}+d_g}}$$

Failure outside the shear-reinforced region

Punching outside the shear-reinforced region occurs if the extension of the reinforced-region from the support is insufficient. In this scenario, diagonal cracks propagate from the tension face down to the bottom end of the shear reinforcements in the outermost perimeter. The resistance for failure outside the shear-reinforced region is expressed as:

10. $$V_{R,out} = \frac{0.75\, b_{0,out} \,.d_v\,.\sqrt{f_c'}}{1+15\frac{\psi.d}{d_{g0}+d_g}}$$

where $b_{0,out}$ is the length of an effective control perimeter positioned at $0.5d$ from the outermost shear reinforcement perimeter (calculated with an upper limit of $3d$ (MC2010) on the maximum tangential spacing between adjacent shear reinforcements) and d_v is the mean effective depth of the flexural tension reinforcement measured from the bottom end of the shear reinforcement.

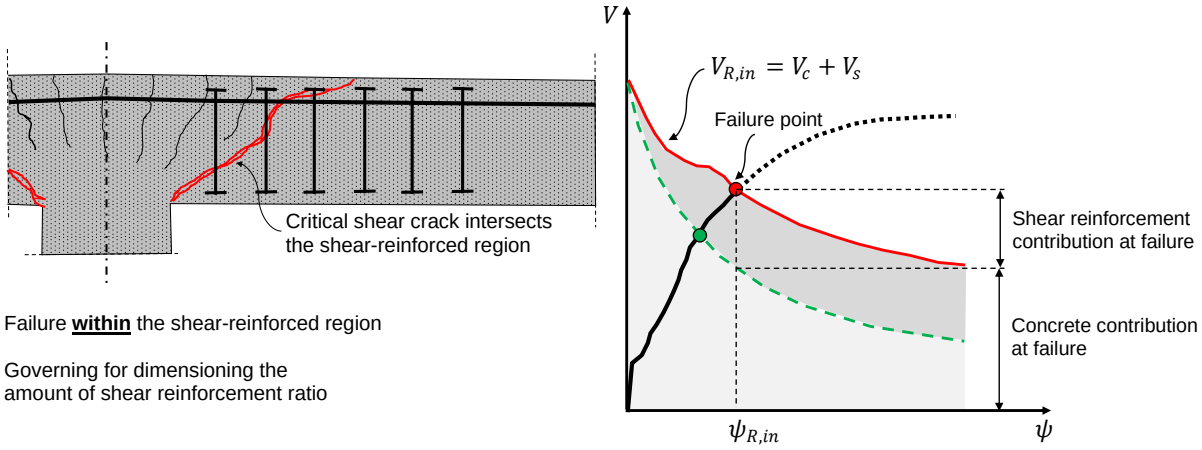


Figure 1. **Punching failure modes of flat slabs with shear reinforcement and their corresponding failure criterion according to the CSCT: (a) failure within the shear-reinforced region; (b) failure due to crushing of concrete strut; (c) failure outside the shear-reinforced region (adapted from Einpaul et al., 2016).**

Nonlinear finite element analysis of slabs with shear reinforcement using 3-D solid element (ATENA)

Introduction

In order to get a better understanding of the mechanics of punching failure in slabs with shear reinforcement, a detailed investigation was carried out using NLFEA with 3-D solid elements in ATENA (Cervenka et al., 2018). Slabs PL7, PL11, and PL12 of Lips et al. (2012) were chosen for simulation due to their widely varying shear reinforcement ratios. All three slabs measured 3000 mm x 3000 mm x 250 mm (effective depth of around 200 mm) and were centrally supported on a 260 mm square steel plate. The flexural reinforcement ratio was around 1.5% in all three slabs. Radially arranged headed studs were used in all three slabs. The first perimeter of studs was placed at a radial spacing (s_0) of 80 mm from the column face. The remaining studs were positioned at consecutive radial spacings (s_1) of 160 mm (radial arrangement) as described below:

a) PL11 had studs of 10 mm diameter arranged in 8 radii ($\rho_t = 0.23\%$ where ρ_t is the shear reinforcement ratio calculated on a perimeter at $d/2$ from the edge of the support region)
b) PL12 had studs of 10 mm diameter arranged in 16 radii ($\rho_t = 0.47\%$)
c) PL7 had studs of 14 mm diameter arranged in 16 radii ($\rho_t = 0.93\%$)

The shear-reinforced region in all three slabs extended to approximately $5.2d$ from the column face to prevent failure outside of the shear-reinforced region. More information regarding the material properties, test setup, and instrumentation can be found in Lips et al. (2012).

Numerical methodology

In ATENA, a smeared crack approach was used in conjunction with concrete material model CC3DNonLinCementitious2 which combines constitutive models for tensile (fracture) and compressive (plastic) behaviour. The Rankine tensile failure criterion was used with exponential softening. In CC3DNonLinCementitious2, triaxial behaviour of concrete in compression is modelled using the Menetrey-William failure surface (Menetrey and William, 1995). The hardening part of the compressive response is expressed in terms of strain while the softening part is expressed in terms of a

limiting displacement w_d at which the compressive stress reduces to zero. This approach is based on the work of Van Mier (1986) and is equivalent to relating the softening response to the compressive fracture energy. After concrete cracks, the compressive strength is reduced in the direction parallel to the cracks similarly to the Modified Compression Field Theory (Vecchio and Collins, 1986). ATENA gives the option of using either a fixed- or rotating-crack model. The latter was used in this study since it was found to give more accurate load-rotation responses than the fixed crack model which tended to overestimate stiffness. A calibration study (Setiawan et al., 2019a) showed that flexural deformation and punching capacity can be captured accurately using 10 linear order (8-noded) brick elements through the slab thickness.

By taking the advantage of symmetry, only a quarter of the slab specimen was modelled. For optimum element aspect ratio, 25 x 25 x 25 mm^3 brick elements were used to model the slab within twice the slab effective depth ($2d$) of the column face while a coarser mesh (50 x 25 x 25 mm^3 and 50 x 50 x 25 mm^3) was used elsewhere. The test apparatus, including support and loading plates, was modelled using linear tetrahedral (4-noded) elements with elastic steel material properties. Both flexural reinforcement bars and headed studs were modelled with embedded 1-D 2-noded linear truss elements with perfect bond. No special measures were taken to anchor the ends of the shear reinforcement using additional truss elements as done by Genikomsou (2015). The stress-strain relationship of the reinforcing bars was assumed to be bilinear with very minimal strain hardening. Vertical loads were applied in load-control using the Arc-Length iteration method. The number of iterations was limited to 100 for each load step. The convergence tolerance was set at 1% for displacement, residual, and absolute residual error and 0.01% for energy error as defined in Cervenka et al. (2018). The key input parameters used in the analyses are summarised in **Table 1**. The concrete parameters are the same as used previously for slabs without shear reinforcement (Setiawan et al. 2019a,b, 2020). Mesh configuration and boundary conditions for the simulated slabs are shown in **Fig. 2**.

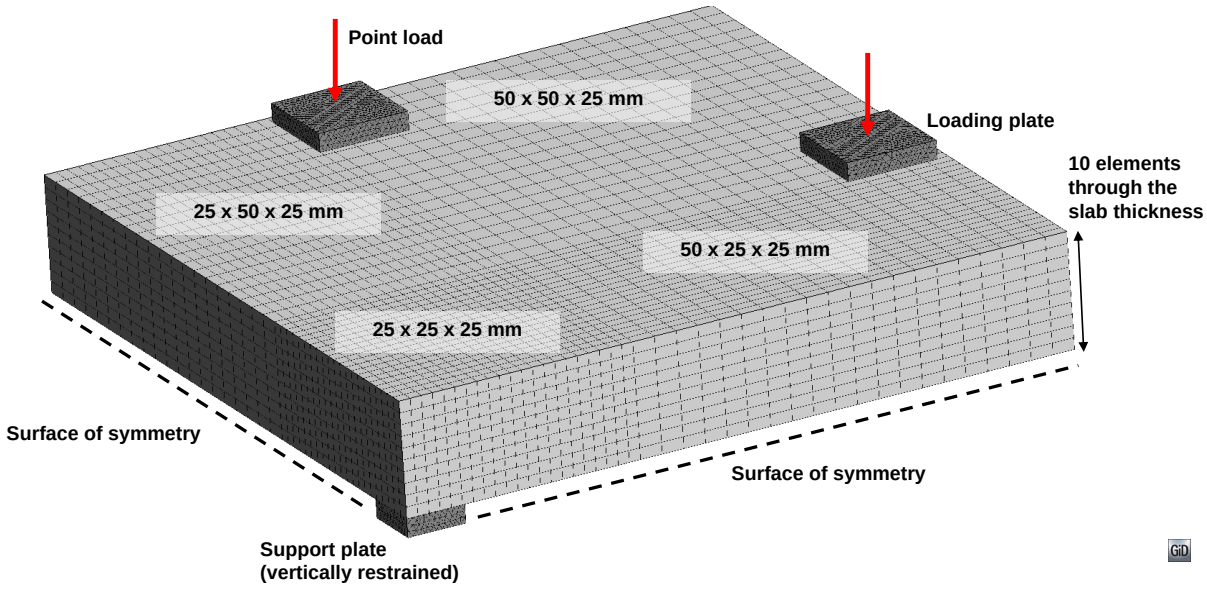
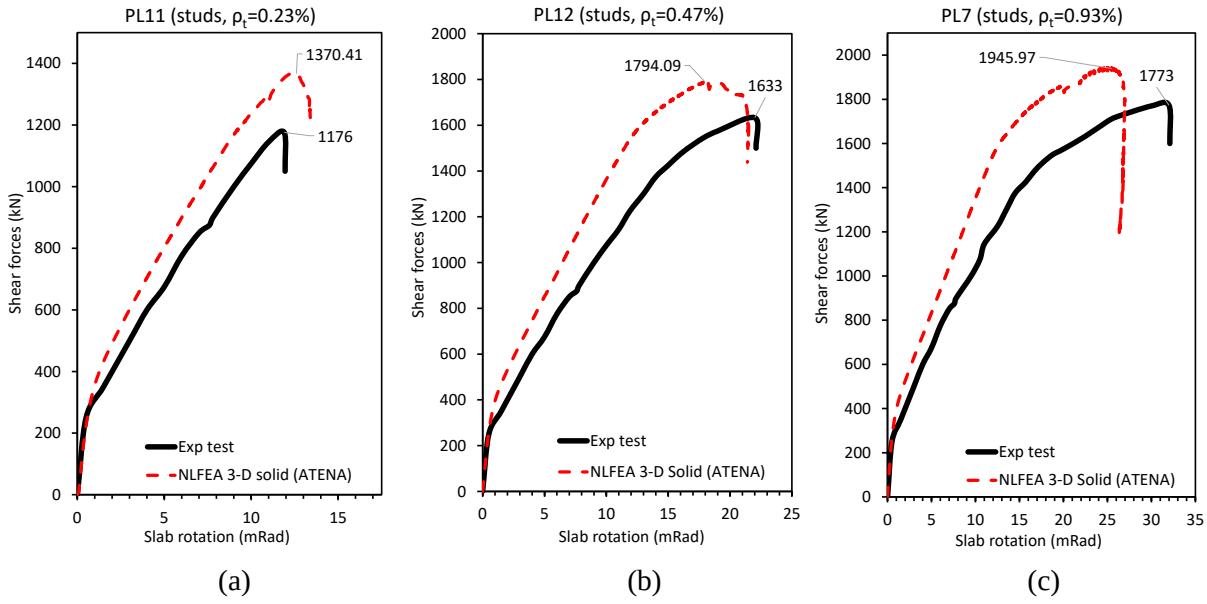


Figure 2. **Mesh configuration and boundary conditions of typical quarter slab model in ATENA.**

NLFEA results

Global responses

The NLFEA was validated at the global level by comparing the predicted versus measured load-rotation response and failure load. **Fig. 3** shows that the punching capacity is reasonably predicted with estimated capacity typically around 10-15% higher than measured.



(a) (b) (c)

Figure 3. **Measured vs predicted load-rotation response and failure load acquired using 3-D solid analysis in ATENA for slabs: (a) PL11 (ρ_t = 0.23%); (b) PL12 (ρ_t = 0.47%); (c) PL7 (ρ_t = 0.93%).**

The predicted load-rotation response is also slightly stiffer than observed experimentally. A possible cause of the strength over-estimation is the assumption of perfect bond between the headed studs and solid concrete. More accurate results could possibly be acquired by explicitly modelling bond-slip and head anchorage of the shear reinforcement but this is beyond the scope of the current study.

Local responses

- **Crack patterns, plots of concrete principal stress-strain, yielding of the headed studs**

Measured and predicted crack patterns and shear reinforcement strains were compared to assess the realism of the NLFEA. Concrete principal strains were also studied. The post-peak strains in **Fig. 4** were extracted when the load had dropped to around 80-90% of its peak value. Typical results are shown in **Fig. 4** for slabs PL12 (ρ_t = 0.47%) and PL7 (ρ_t = 0.93%). Both slabs failed in punching with PL12 failing within the shear-reinforced region and PL7 failing due to strut crushing. The following conclusions are drawn from **Fig. 4**:

1) The NLFEA broadly captures the observed crack patterns but differences between the crack patterns in PL12 and PL7 are less marked for the NLFEA than experimentally observed.
2) The positions of peak tensile strain in **Fig. 4** coincide with the positions of maximum crack width. The peak tensile strain is located further from the support in PL12 than PL7 which is consistent with the experimentally observed cracking patterns but the peak strain is more concentrated over the support in PL7 than observed in reality. The diagonal contours of principal compressive stress are indicative of strut action.
3) Comparison of strains in the shear studs of PL12 (**Fig. 4(a)**) shows that ATENA predicts studs to yield at their bottom end in the 1st perimeter and at the top end in the 2nd perimeter. In the test, the 1st perimeter almost reached yield where predicted but the 2nd perimeter yielded at the top and bottom ends rather than just the bottom as predicted. In slab PL7 (**Fig. 4(b)**), ATENA correctly predicts studs to yield in the 1st and 2nd perimeters with much lower stress in the 3rd perimeter as observed. However, the observed yielding at the top end of the 1st perimeter is not predicted. These observations suggest that, due to the assumption of perfect bond, yielding of the shear reinforcement was more localised in the NLFEA than in reality.

On the basis of these observations it is concluded that the 3-D solid model adequately captures the experimentally observed failure modes of PL7 and PL12.

- **Contribution of concrete and headed studs as a function of slab rotation**

This section compares the measured and predicted forces resisted by the concrete (V_c) and shear reinforcement in the 1st ($V_{w,1\ bot}$) and 2nd perimeters ($V_{w,2\ top}$). Lips (2012) determined $V_{w,1\ bot}$ and $V_{w,2\ top}$ from strains measured in the bottom and top ends of the first and second perimeters of studs respectively. The concrete contribution V_c was subsequently acquired by subtracting $V_{w,1\ bot} + V_{w,2\ top}$ from the support reaction. This procedure was used to assess the NLFEA apart from $V_{w,1\ bot}$ and $V_{w,2\ top}$ being calculated in terms of maximum strain along the shear reinforcement. **Fig. 5** compares the resulting predicted forces in PL7 and PL12 with those determined experimentally by Lips. The vertical and horizontal axes in **Fig. 5** are expressed in terms of normalised shear stress and normalised rotation respectively expressed as:

11. $v_{norm} = \frac{V_c\ or\ V_{w,1\ bot}\ or\ V_{w,2\ top}}{b_0.d.\sqrt{f_c'}}$

12. $\psi_{norm} = \frac{\psi.d}{d_{g0}+d_g}$

Fig. 5(a) and **(b)** show that ATENA gives reasonably accurate predictions of the individual contributions to shear resistance for both slabs but the stud contribution is slightly higher than measured. This may be the case since maximum strains were used in ATENA analysis whereas, in the tests, strain was only measured at the bottom and top ends. Nevertheless, consideration of **Fig. 5** shows that the ATENA analysis captures the following key aspects of the experimentally observed behaviour:

1) The concrete contribution is dominant at low slab rotations but gradually decreases with increasing slab rotation as assumed by the CSCT.

2) The concrete contribution reduces more rapidly with slab rotation in PL7 than PL12. Furthermore, V_c makes a small yet significant contribution to the peak shear resistance of PL12 (around 25%) but not to the peak resistance of PL7. The latter conclusion is dependent on the assumption that two perimeters of shear reinforcement contribute to resistance which is debatable given the steep inclination of the critical shear crack of PL7.

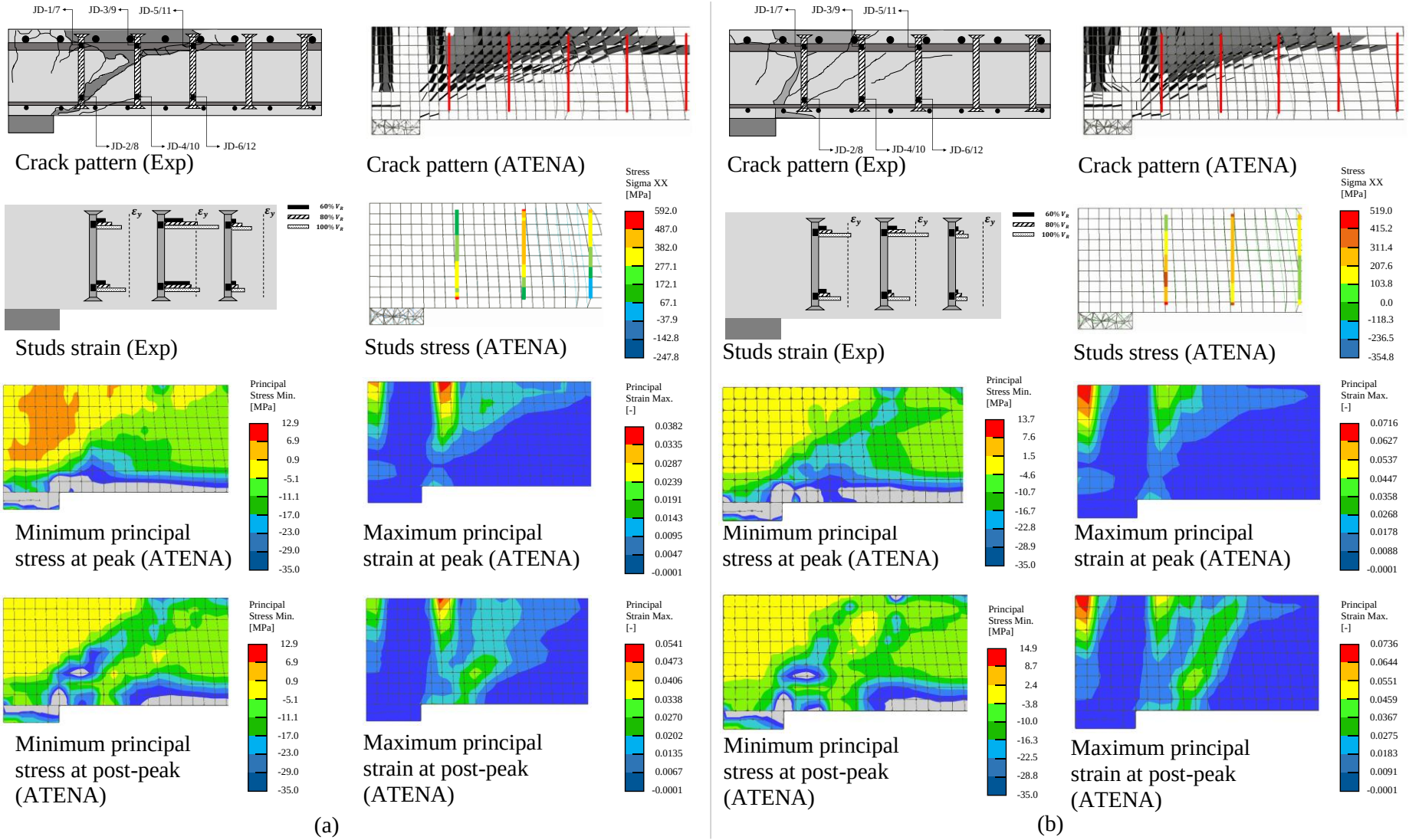
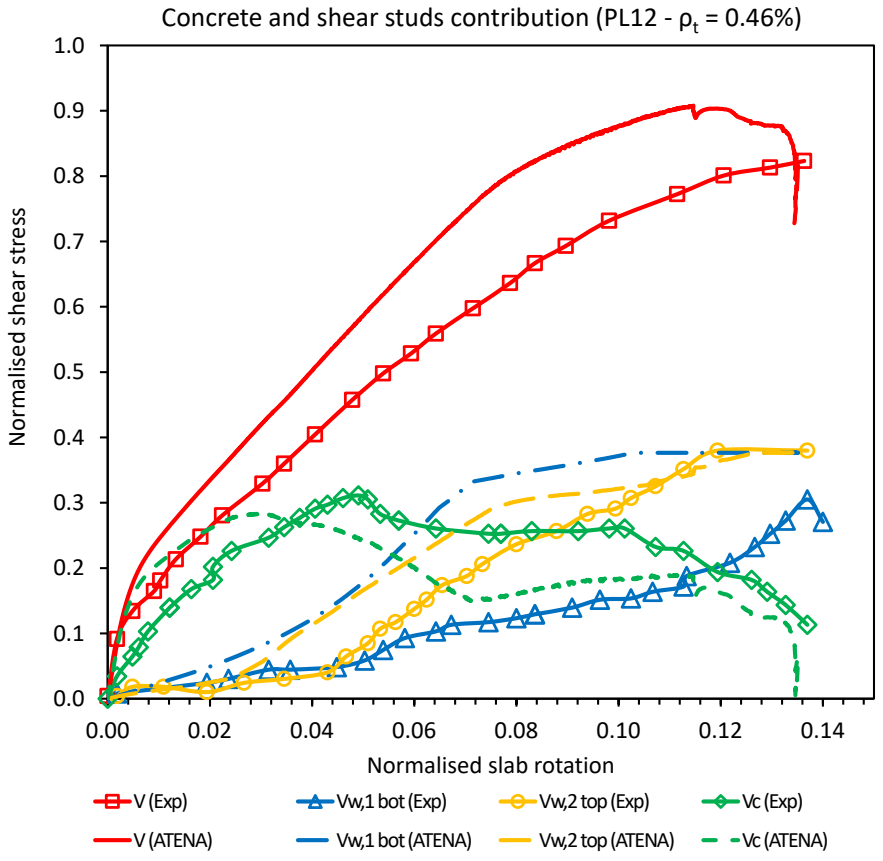
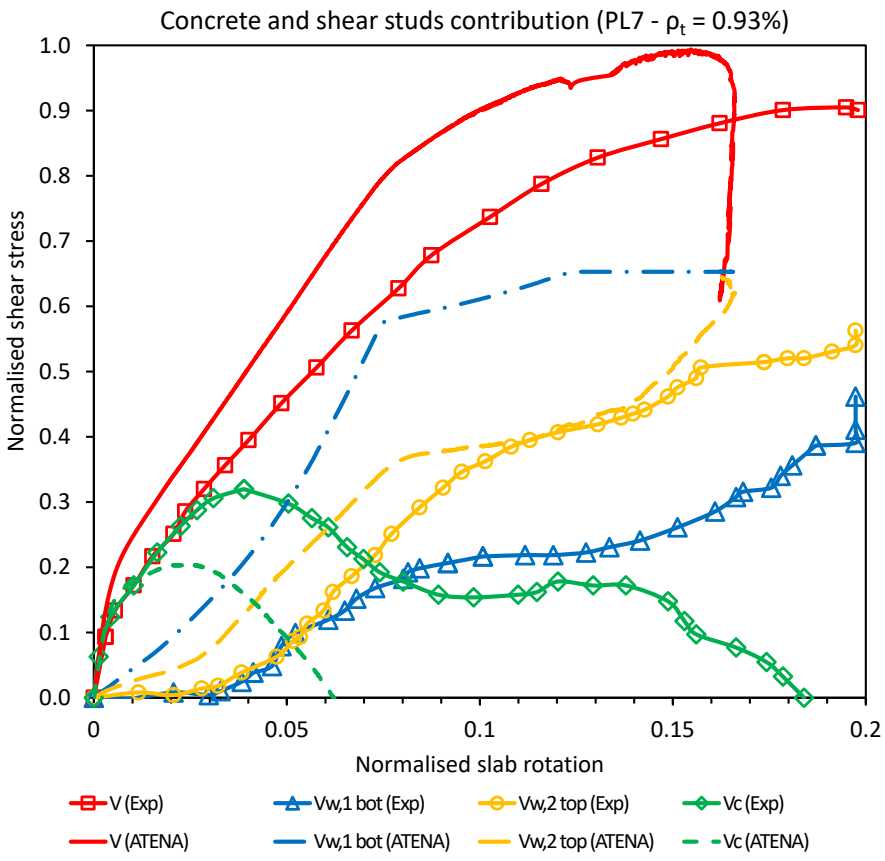


Figure 4. **Measured vs predicted crack pattern (crack width > 0.1 mm), stress-strain of headed studs, minimum concrete principal stress and maximum concrete principal strain of slabs: (a) PL12; (b) PL7.**



(a)



(b)

Figure 5. Individual contribution of concrete (V_c), 1st and 2nd layer of headed studs ($V_{w,1\ bot}$ and $V_{w,2\ top}$) of slabs: (a) PL12; (b) PL7.

- **Activation of shear reinforcement at each individual perimeter**

The percentage activation (S_{act}) of each perimeter of shear reinforcement was calculated, at each load step, as follows to examine its relationship to shear reinforcement ratio (ρ) and failure mode.

13. $S_{act}\ (\%) = \frac{\sum_{i=1}^{n_r} A_s.f_{sji_{max}}}{n_r A_s.f_{yw}} \leq 100\%$

where n_r indicates the number of radii of shear reinforcement, A_s is the cross-sectional area of a single shear stud, $f_{sji_{max}}$ is the maximum stress in shear stud *i* of perimeter j extracted from ATENA and f_{yw} is the yield strength of the headed studs.

Fig. 6 shows the activation of studs in each perimeter for slabs PL11, PL12, and PL7. The horizontal axis shows the applied load as a proportion of the predicted peak load (P_u) while the vertical axis shows the % shear reinforcement activation in each perimeter. **Fig. 6(a)** shows that in slab PL11, with the lowest shear reinforcement ratio, the first two perimeters of studs fully yielded at failure. A similar pattern is observed in slab PL12 (see **Fig. 6(b)**), but with less stress developing in the 3rd and 4th rows. On the other hand, for slab PL7 (**Fig. 6(c)**) where failure was due to crushing of concrete struts, studs only yielded in the 1st row with relatively low stresses developing in the 2nd - 4th rows compared with PL11 and PL12 (see **Fig. 6(c)**). In all three slabs, stresses in the 5th - 7th rows were practically negligible. The reduced activation of shear reinforcement in the second perimeter of PL7 compared with PL11 and PL12 is consistent with the experimentally observed steep inclination of the critical shear crack.

These validation studies show that the ATENA analysis is capable of realistically simulating punching failure of slabs with shear reinforcement. However, the very computationally demanding nature of the analysis restricts its application to the analysis of simplified test specimens and sub-assemblages. To circumvent this, Setiawan et al., (2019b) developed the so-called Joint-Shell Punching Model (JSPM) for modelling punching and post-punching (Fernandez Ruiz et al., 2013) failure in slabs without shear reinforcement. The JSPM, which is implemented in the nonlinear structural analysis program ADAPTIC (Izzuddin, 1991), models punching failure with joint elements inserted between the nodes of nonlinear shell elements. The proposed approach has some similarities with the earlier work of Keyvani et al. (2014) and Liu et al. (2015a,b) but the connector shear resistance is defined more systematically in the JSPM. Both the earlier studies focussed on assessing the global behaviour of flat

slab buildings failing in punching. In each case, the shear resistance of the connector elements adopted in the global analysis was predetermined from analysis of concentrically loaded isolated internal column punching specimens. As acknowledged by Liu et al. (2015b), this treatment neglects the increase in punching resistance which occurs as the line of contraflexure moves in towards the column, producing a stiffer response, as the slab is loaded beyond cracking and yielding. The advantage of the proposed approach over those of Keyvani et al. and Liu et al. is that the joint shear resistance is calculated at each load step, in terms of the slab kinematics, rather than having to be predetermined in advance. Unlike the other two methods, the proposed approach also models shear redistribution of the type identified by Sagaseta et al. (2011) which can significantly enhance punching resistance particularly when loading or geometry is non-axis-symmetrical. This paper extends the application of the JSPM to shear reinforcement.

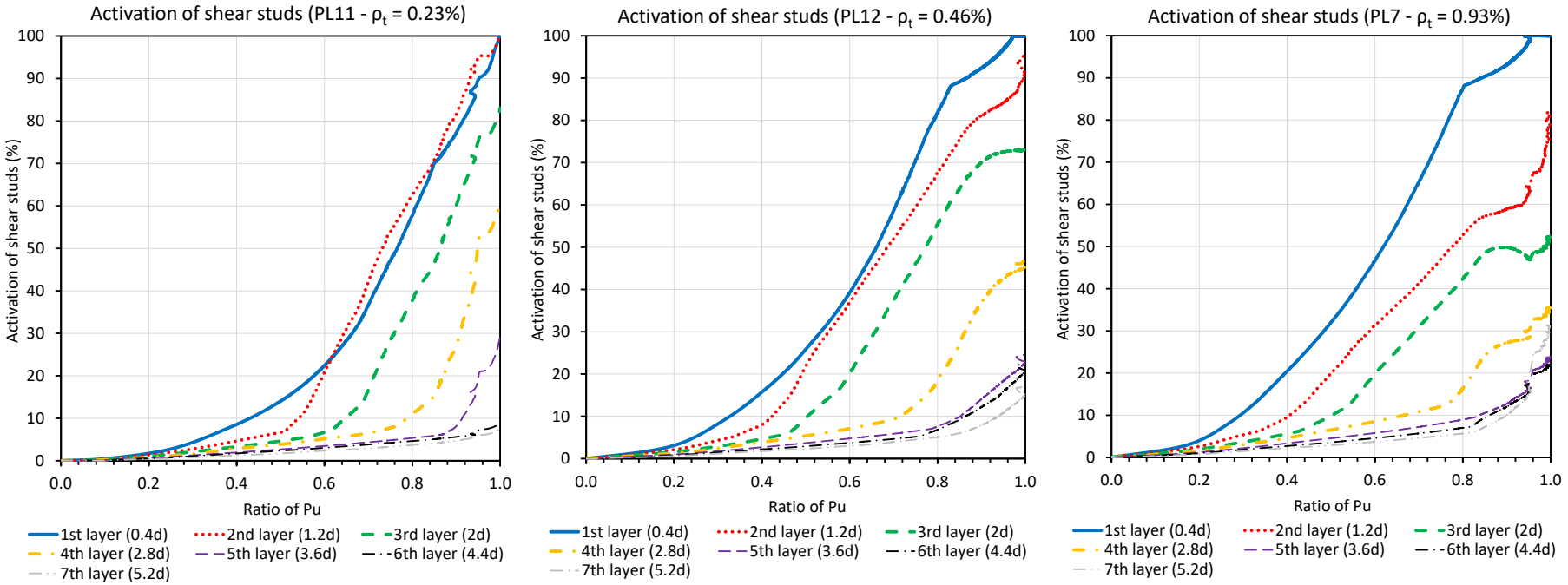


Figure 6. Activation of shear studs at each individual layer of studs predicted from NLFEA (ATENA) for slabs: (a) PL11; (b) PL12; (c) PL7.

Extension of the JSPM algorithm to consider the contribution of shear reinforcement

Brief review of the original JSPM for slabs without shear reinforcement

The JSPM (Setiawan et al. 2019b) models flexural behaviour with nonlinear layered-shell elements (Izzuddin et al. 2004) whilst simulating punching failure by means of nonlinear joint elements positioned around a control perimeter located at $0.5d$ from the column. The shear resistance of individual joint elements is calculated using the critical shear crack theory (CSCT) of Muttoni (2008). The adopted joint element, depicted *jel3* (Izzuddin, 1991), has two initially coincident nodes (nodes 1 and 2). Punching failure is simulated through separation of these nodes in the out-of-plane direction of the slab. The JSPM includes a novel feature whereby monitoring points (defined as nodes 3 and 4 in **Fig. 7**) can be paired with the joint element to inform it of the slab and column chord rotations. Each joint element has an imaginary sector element associated with it (see **Fig. 7(a)** and **(c)**) within which node 3 of the joint element is positioned. The shear resistance of each individual joint is related to the relative slab-column rotation within its sector. This is given by the difference in rotation between nodes 3 and 4. For a best fit with experimental observations, node 3 is positioned at a radius of around $0.22L$ from the column centreline (where L is the slab span between column centrelines) as recommended by Soares and Vollum (2015). In continuous slabs, the radius of $0.22L$ corresponds to the line of radial contraflexure for symmetric loading. For isolated slab specimens tested in laboratory, node 3 is positioned around the slab free edges where radial curvature is minimal.

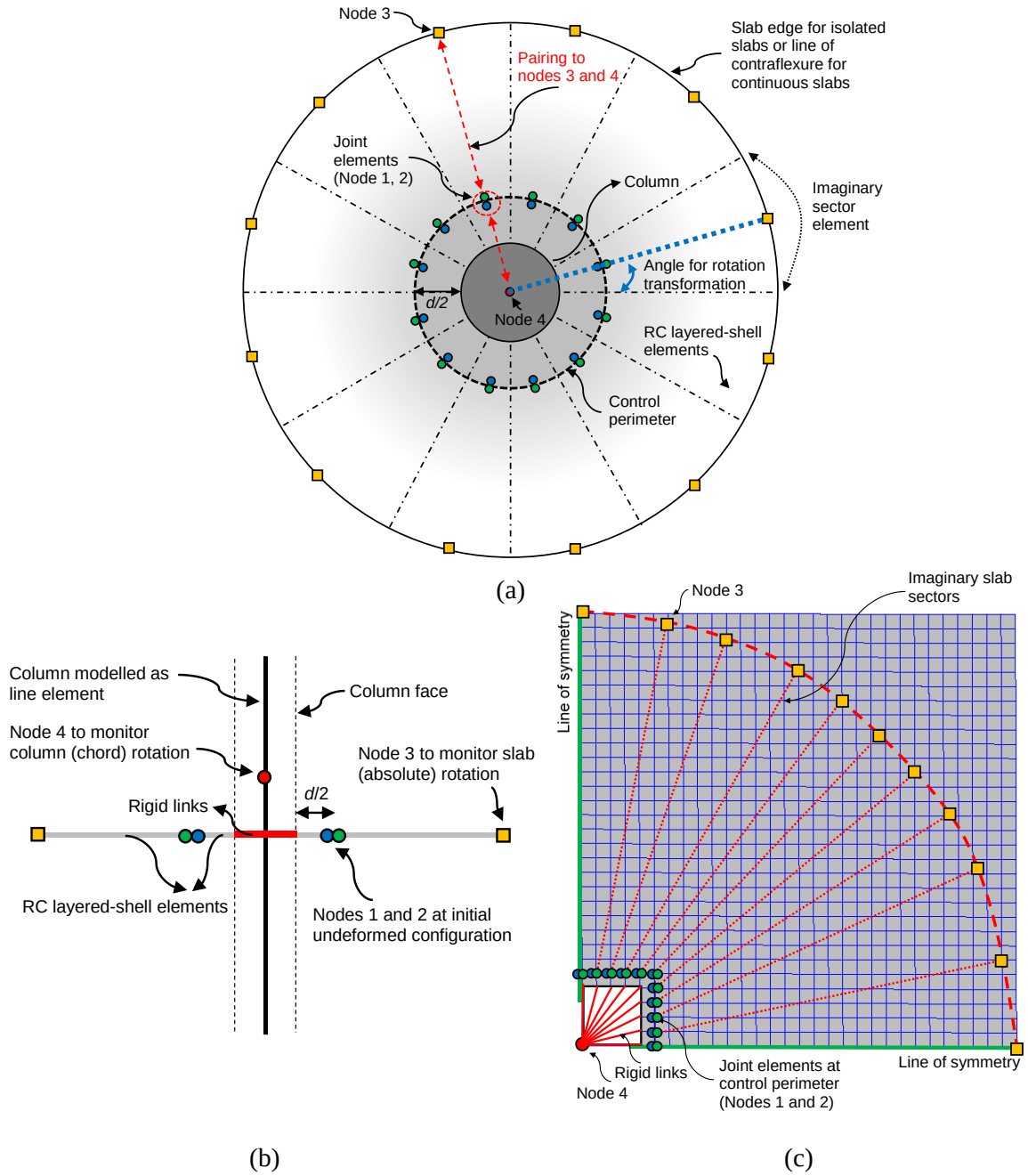


Figure 7. **Illustration of the proposed modelling strategy: (a) plan view; (b) elevation view; (c) implementation of the JSPM along with pairing system of monitored nodes in ADAPTIC for a quarter slab model.**

The constitutive behaviour of the joint element in the out-of-plane direction consists of three main phases: 1) linear-elastic; 2) local joint failure and shear redistribution and 3) post-punching. Transition from phase 1) to 2) occurs when joint shear force first reaches its shear resistance calculated according to the CSCT. After the failure criterion is violated, phase 2) is entered and the joint shear force decreases following the shape of the CSCT curve as proposed by Sagaseta et al. (2011). This results in shear force being redistributed from failing joint elements to adjacent joint elements yet to fail. This process

continues until failure is detected in all joint elements after which phase 3) is entered. In phase 3), joint resistance decreases abruptly to a constant value equal to the post-punching resistance determined according to Fernandez Ruiz et al. (2013). This provides a lower estimate of the post-punching strength which, in reality, can increase significantly with larger deflections as shown in Fernandez Ruiz et al (2013). **Fig. 8** shows the complete constitutive relationship (phase 1 - 3) of the joint element in out-of-plane direction. Globally, phases 2 and 3 always happen sequentially with no overlap between the two. This ensures that all the joint shear forces during the redistribution phase (phase 2) are solely controlled by the CSCT failure criterion. In the proposed algorithm, the transition from phase 2 to phase 3 is controlled by a joint displacement threshold which is chosen to be sufficiently large that no joint enters phase 3 prior to all joints entering phase 2.

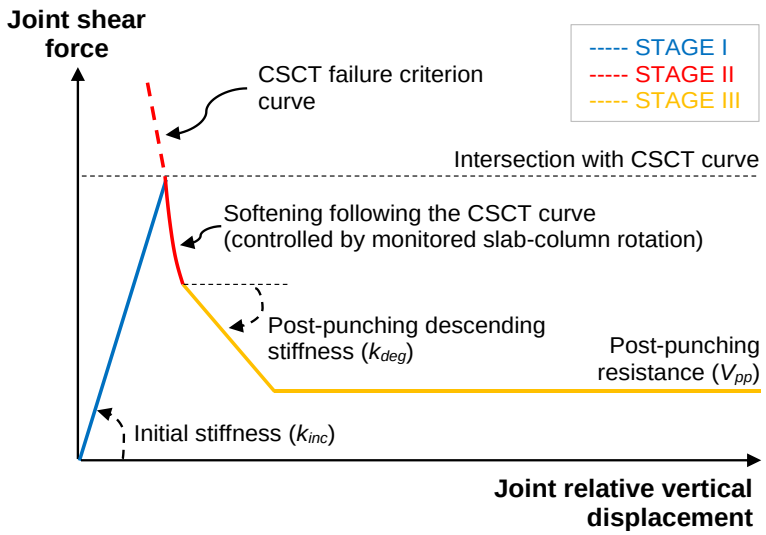


Figure 8. Proposed joint force-deformation relationship in out-of-plane DOF.

Contribution of shear reinforcement

The JSPM was extended to calculate the punching resistance of slabs with shear reinforcement failing inside the shear reinforced zone as described in the flowchart shown in **Fig. 9**. Both failure inside the shear reinforcement and strut crushing are considered in the extended model which is depicted JSPMS. It would be necessary to add a further perimeter of joints to consider failure outside the shear-reinforced zone.

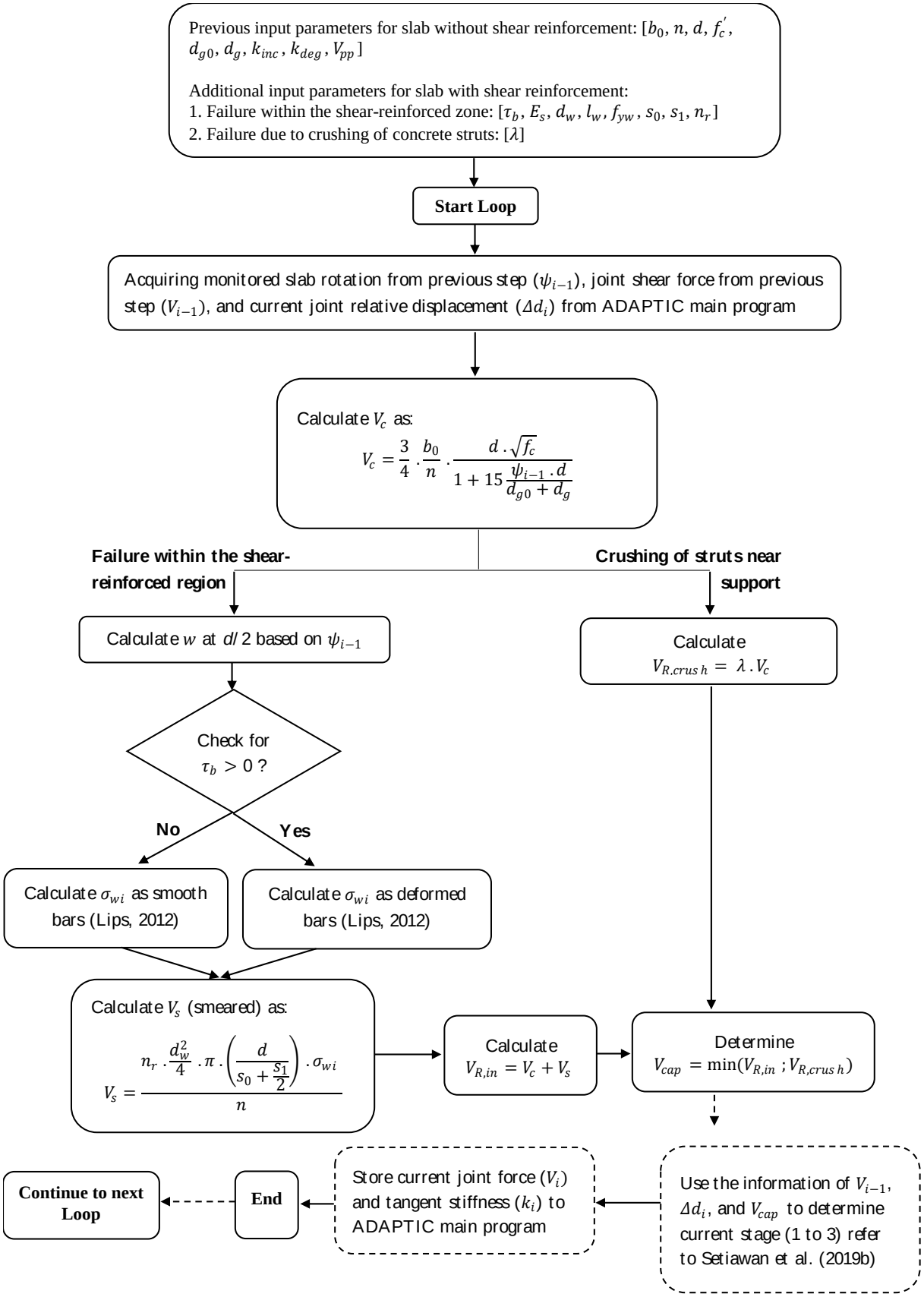


Figure 9. Extended JSPM algorithm to include the contribution of shear reinforcement according to CSCT (Fernandez Ruiz and Muttoni, 2009).

Verification of the JSPMS for isolated slabs with shear reinforcement

The JSPMS was validated using the three previously considered slabs from the test series of Lips et al. (2012) as well as five slabs with stirrups tested by Chana and Desai (1992a). Both test setups consisted of isolated specimens intended to simulate punching at internal slab column connections.

One quarter of each slab of Lips was modelled in ADAPTIC using a uniform mesh size of 50 mm x 50 mm. The support plate was modelled by restraining the shell element nodes vertically within the support region. External load was initially applied in force-control and thereafter in displacement-control. Newton-Raphson iteration was used in the first phase followed by the Arc-Length method in the second phase. The convergence criteria were chosen based on the work reference (energy norm) with 10 iterations limit for each load step. The material properties for the concrete and reinforcement bars were as described previously (Izzuddin et al., 2004; Elghazouli and Izzuddin, 2004; Setiawan et al., 2019b). The multiplier λ used to calculate maximum possible punching resistance was taken as 3.0 for slabs with headed studs as suggested by Fernandez Ruiz and Muttoni (2009). **Fig. 10** shows a typical slab modelled in ADAPTIC along with its mesh configuration and boundary conditions.

Five slabs from Chana and Desai (1992a) were modelled, namely specimens: 2, 4, 5, 8, and 9. All five slabs had the same plan dimensions of 3000 mm x 3000 mm but varying slab thickness (228; 240; 250 mm) and column size (300 x 300; 400 x 400 mm). The flexural reinforcement ratio was around 0.8-0.85%. All five slabs had similar orthogonal stirrup arrangements with the first perimeter installed at $0.5d$ from the column face. Further rows were located at $1.25d$, $2.0d$, and $2.75d$, hence giving s_0 = $0.5d$ and s_1 = $0.75d$. The number of stirrups per perimeter varied as follows in the first two perimeters:

1) Specimen no. 2: 1st perimeter = 12; 2nd perimeter = 12
2) Specimen no. 4: 1st perimeter = 24; 2nd perimeter = 24
3) Specimen no.5: 1st perimeter = 12; 2nd perimeter = 20
4) Specimen no.8: 1st perimeter = 12; 2nd perimeter = 20
5) Specimen no.9: 1st perimeter = 20; 2nd perimeter = 28

The effective area of shear reinforcement (smeared) within b_0 for the calculation of V_s in the JSPMS was determined as:

14. $A_{s-total} = A_{st1} + A_{st2}$

with

15. $A_{st1} = \left(n_{r1}.\frac{\pi.d_w^2}{4}\right)$

16. $A_{st2} = \left(n_{r2}.\frac{\pi.d_w^2}{4}\right).\left(\frac{d}{s_0+\frac{s_1}{2}} - 1\right)$

where A_{st1} and A_{st2} are the total areas of shear reinforcement (smeared) within the 1st and 2nd perimeters respectively, n_{r1} and n_{r2} are the number of stirrups in the 1st and 2nd perimeters respectively. In ADAPTIC, only quarter of the slab was modelled with a uniform mesh size of 50 mm x 50 mm. The λ factor was taken as 2.0 for all isolated slabs with stirrups as suggested by Fernandez Ruiz and Muttoni (2009).

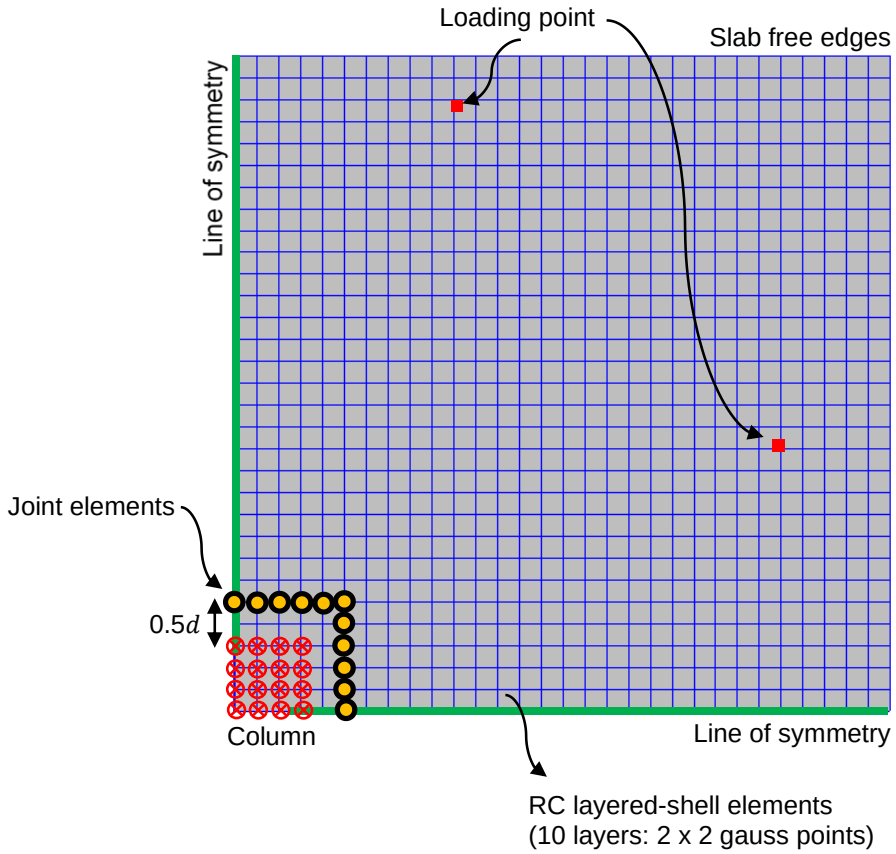


Figure 10. Quarter of typical slab from Lips et al. (2012) modelled in ADAPTIC along with its mesh configuration and boundary conditions.

Fig. 11 and **12** show the predicted load-rotation responses for the slabs of Lips et al. (2012) and Chana and Desai (1992a) respectively. The measured failure load and CSCT failure criteria for $V_c, V_{R,crush}$, and $V_{R,in}$ are also shown. Results acquired with the 3-D solid analysis are also plotted in **Fig. 11** for the

slabs of Lips et al. (2012). **Fig. 11** shows that JSPMS predicts PL11 and PL12 to fail within the shear-reinforced region and PL7 to fail due to crushing of struts, as observed experimentally. The failure mode was not reported by Chana and Desai (1992a) so no comparison of actual and predicted failure mode is possible. Overall the JSPMS gives good predictions of measured failure loads as expected since the CSCT also gives good predictions for these slabs.

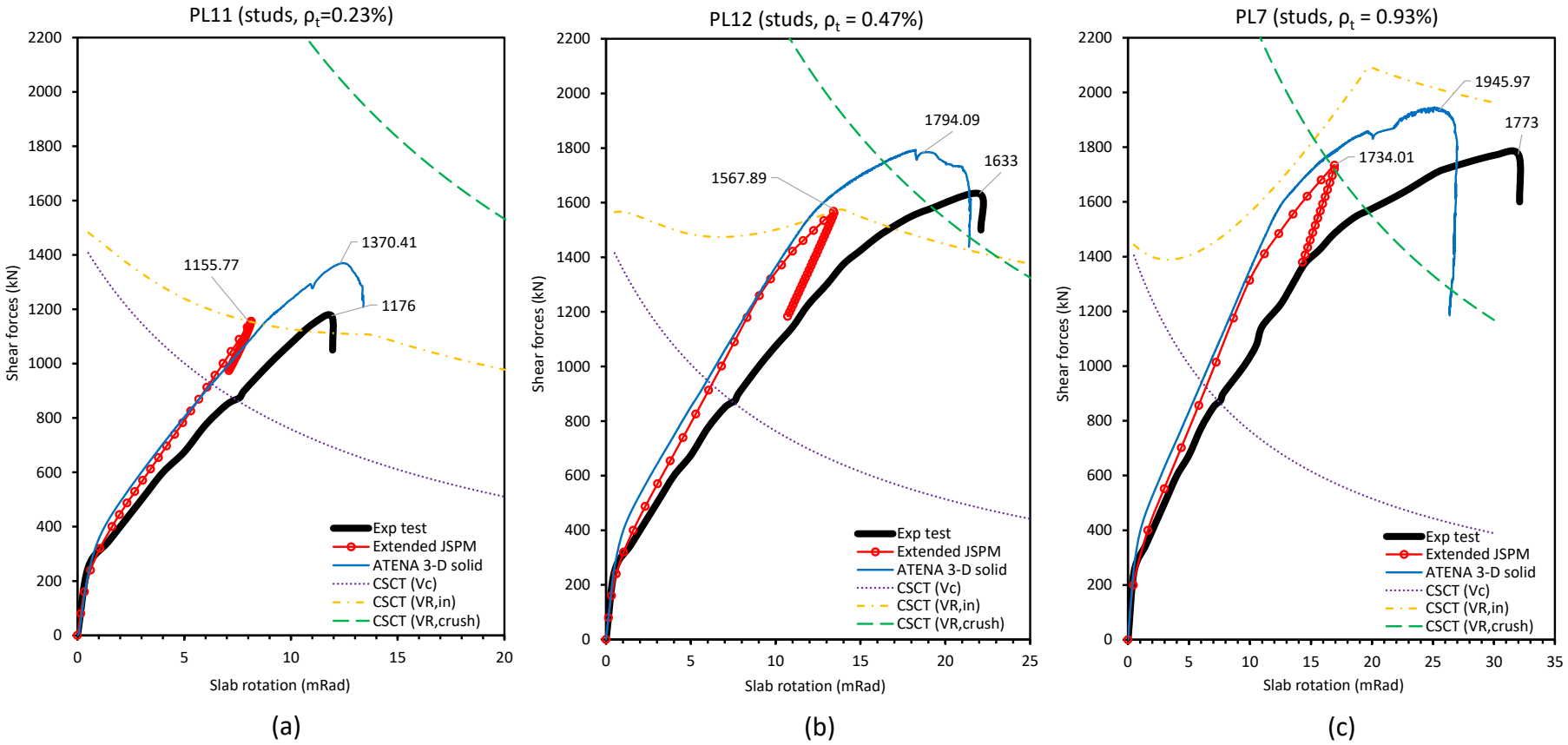


Figure 11. **Load-rotation response and failure load acquired using the extended JSPM of isolated slabs reinforced with headed studs: (a) PL11; (b) PL12; (c) PL7.**

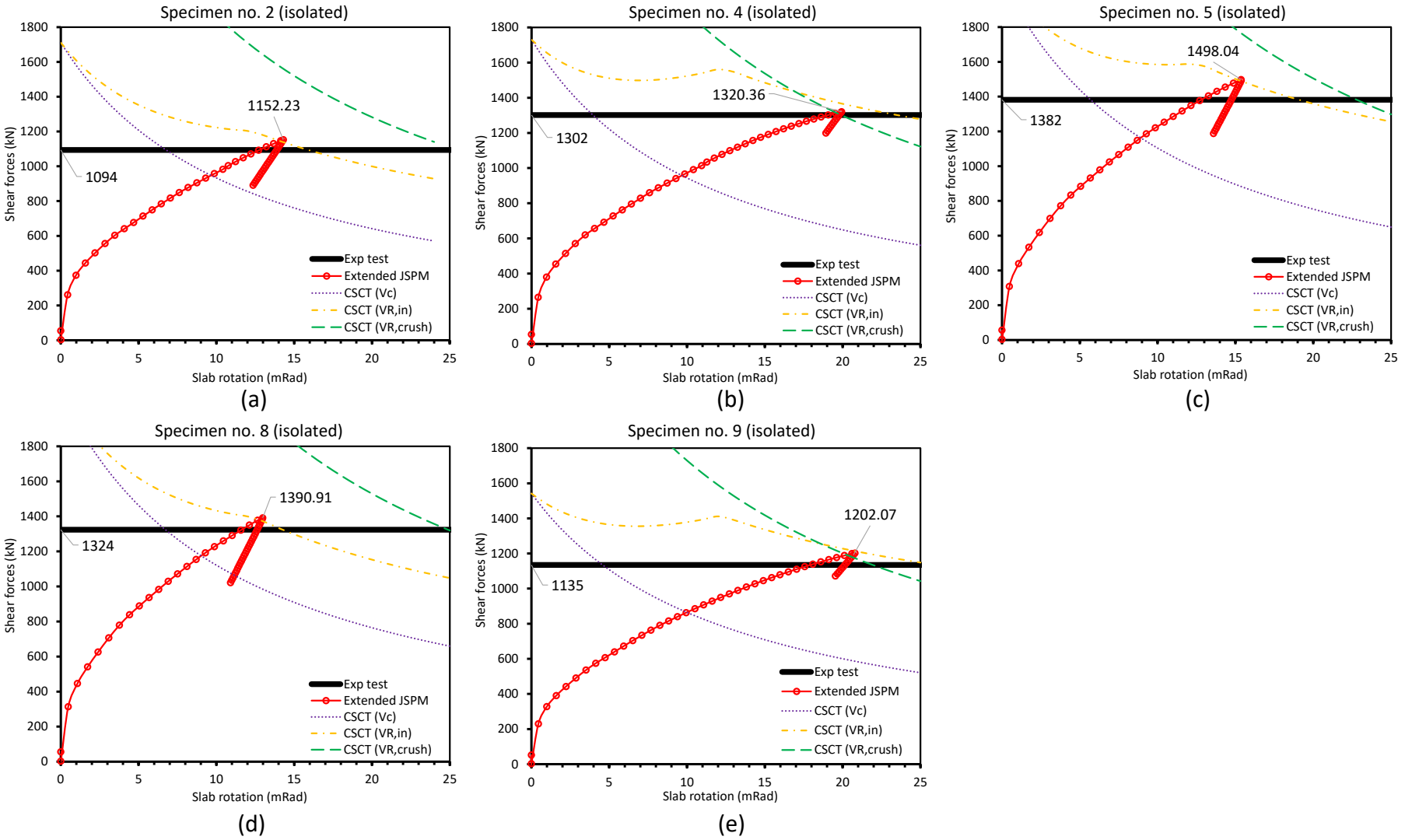


Figure 12. **Load-rotation response and failure load acquired using the extended JSPM of isolated slabs reinforced with stirrups, Specimen no: (a) 2; (b) 4; (c) 5; (d) 8; (e) 9.**

Verification of the JSPMS for continuous slabs with shear reinforcement

As a final verification, the JSPMS was used to analyse four continuous slabs with shear reinforcement (FPS2-5) tested by Chana and Desai (1992b). All four slabs measured 9000 mm x 9000 mm x 250 mm, with effective depth of 210 mm, and were supported on a 400 mm square column. The flexural reinforcement ratio was 0.86% in all slabs. The stirrup positions were the same as in the isolated slabs of Chana and Desai (1992a). Numbers of stirrups in the 1st and 2nd perimeters for each slab were as follows:

1) Specimen FPS2: 1st perimeter = 12; 2nd perimeter = 12
2) Specimen FPS3: 1st perimeter = 8; 2nd perimeter = 12
3) Specimen FPS4: 1st perimeter = 16; 2nd perimeter = 24
4) Specimen FPS5: 1st perimeter = 20; 2nd perimeter = 28

All four edges of each specimen were simply supported on a slip membrane laid on blockwork. Load was applied by means of eight symmetrically positioned hydraulic jacks located around a circle with diameter of 2.4 m (see **Fig. 13**). In ADAPTIC, only one quarter of the slab was modelled using a uniform mesh size of 100 mm x 100 mm. The λ factor was taken as 2.0 for these slabs as recommended by Fernandez Ruiz and Muttoni (2009) for stirrups.

Fig. 14 shows the predicted load-rotation response for all the slabs along with the experimental failure load and the CSCT failure criteria. The JSPMS is seen to perform well with predicted resistances slightly lower than measured except for specimen FPS2. Comparison of **Fig. 14** and **Fig. 12** shows that the predicted shear reinforcement contribution (V_s) is much greater in the isolated than continuous slabs due to the larger slab rotation at failure. Ratios of measured/predicted punching capacity (V_{test}/V_{calc}) are presented in **Table 2** for the JSPMS (all slabs) as well as ATENA 3-D (slabs PL11, PL12, and PL7). The JSPMS is seen to be particularly accurate with mean and coefficient of variation of V_{test}/V_{calc} equal to 1.006 and 7.30% respectively.

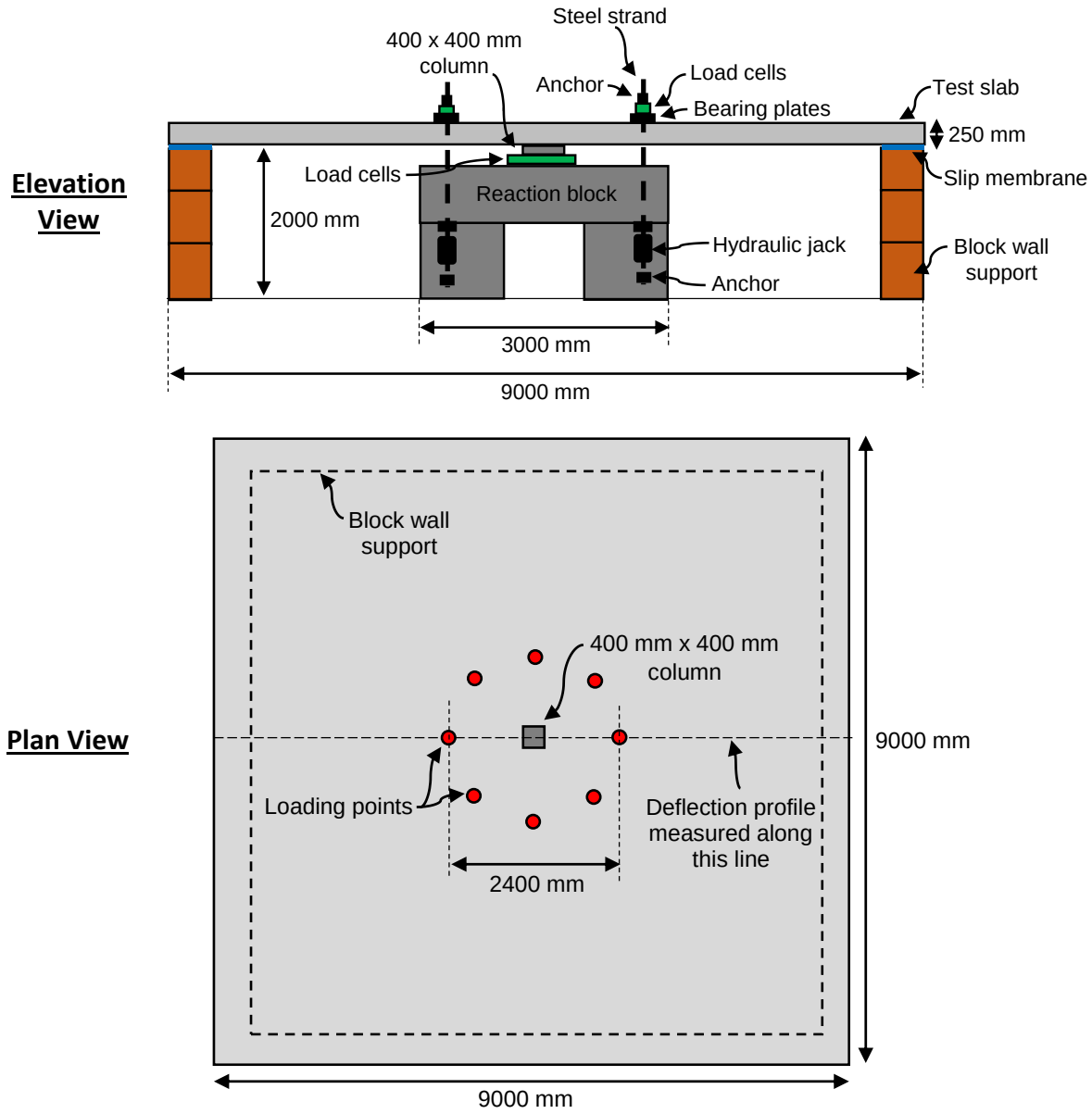


Figure 13. **Experimental test setup for continuous slabs with simple support along edges (adapted from Chana and Desai, 1992b).**

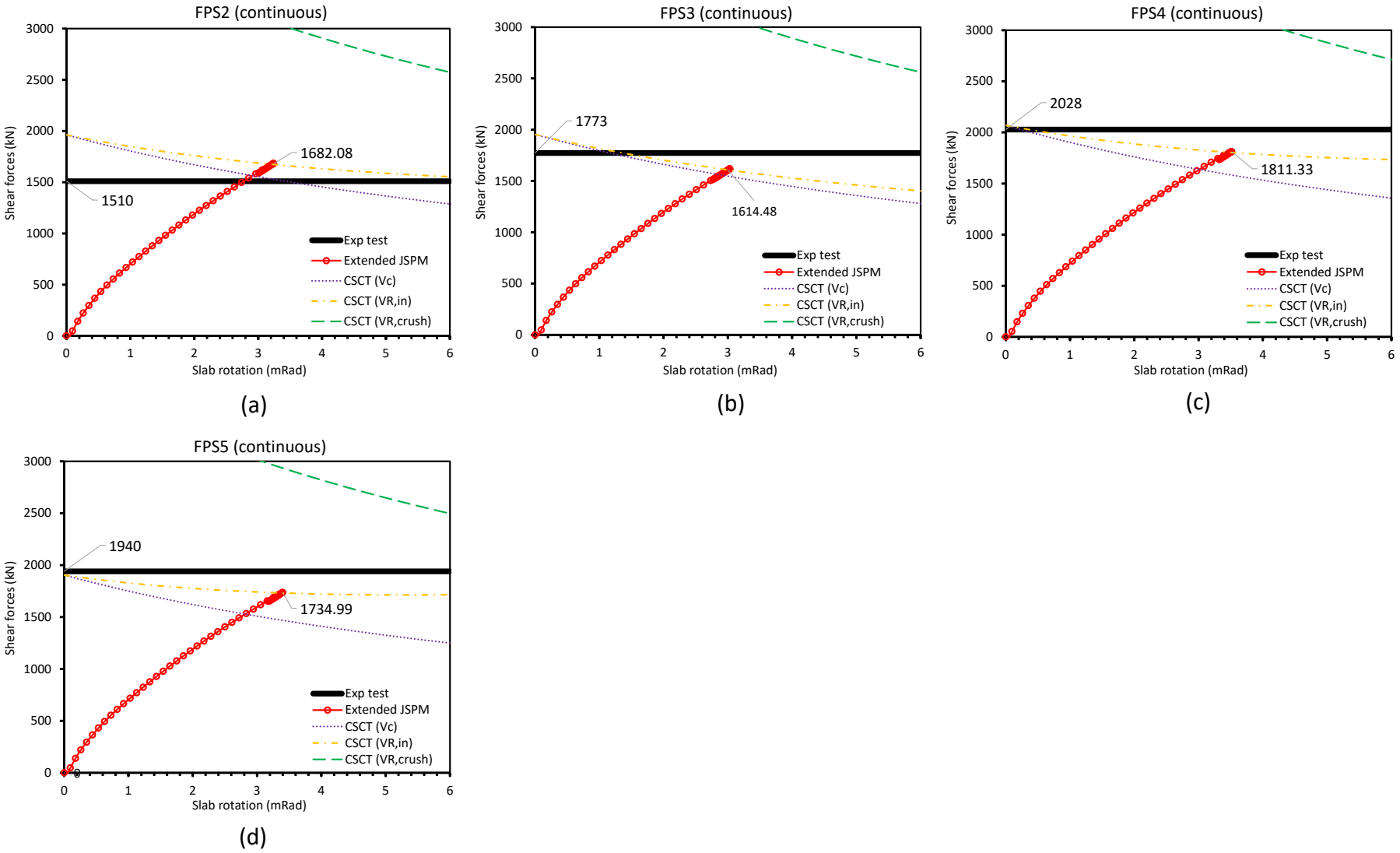


Figure 14. **Load-rotation response and failure load acquired using the extended JSPM of continuous slabs reinforced with stirrups: (a) FPS2; (b) FPS3; (c) FPS4; (d) FPS5.**

Conclusion

This paper presents a detailed numerical investigation into punching shear failure of RC flat slabs with shear reinforcement. NLFEA with ATENA using 3-D solid elements is shown to broadly capture the experimentally observed behavior of three slabs with shear reinforcement tested by Lips et al. (2012). The predicted failure load is slightly higher than the measured punching capacity possibly due to the assumption of perfect bond for shear reinforcement. The NLFEA with solid elements realistically simulates the experimentally observed internal crack patterns along radial saw-cuts as well as the influence of shear reinforcement ratio of the percentage activation of shear reinforcement in each perimeter. The solid element analysis also captures the experimentally observed decrease in concrete contribution (V_c) with increasing slab rotation.

NLFEA with solid elements gives useful insights into punching failure as described above but is overly computationally demanding for general use. To address this the authors have developed a novel Joint-Shell Punching Model (JSPM) in which 3-D joint elements are combined with nonlinear shell elements. This paper extends the application of the JSPM to slabs with shear reinforcement. Punching failure is modelled with joint elements positioned around a control perimeter located at $0.5d$ from the column face (where d is the slab effective depth). The joint shear resistance is calculated at each load step in terms of the slab rotation using the CSCT (Fernandez Ruiz and Muttoni, 2009). The key novelty of the JSPM over previous implementations of the CSCT is that the failure load is calculated internally within the NLFEA without the need for post processing. Furthermore, it also considers shear redistribution of the type identified by Sagaseta et al. (2011) which can significantly enhance punching resistance particularly when loading or geometry is non-axis-symmetrical. The extended JSPM (depicted JSPMS) is shown to give good predictions of punching resistance for both isolated and continuous slabs (V_{test}/V_{calc} = 1.006 with CoV = 7.30%).

Acknowledgement

The work presented in this article was supported by the Indonesia Endowment Fund for Education (LPDP). The opinions and conclusions in this document are those of the authors, and do not necessarily represent those of the sponsors.

References

ACI Committee 318. 2014. *ACI Building Code Requirements for Structural Concrete (ACI 318-14) and Commentary (ACI 318R-14)*. American Concrete Institute, Farmington Hills, MI, 519 pp.

Beutel, R. and Hegger, J. 2002. *The effect of anchorage on the effectiveness of the shear reinforcement in the punching zone*. Cement & Concrete Composites, 24: pp. 539-549.

Birkle, G. and Dilger, W. H. 2008. *Influence of slab thickness on punching shear strength*. ACI Structural Journal, 105(2): pp. 180–188.

BSI. 2004. *BS EN 1992-1-1:2004: Eurocode 2, design of concrete structures – part 1-1: general rules and rules for buildings*. BSI, London, UK.

Cervenka, V., Jendele, L. and Cervenka, J. 2018. *ATENA Program Documentation, Part 1, Theory*. Cervenka Consulting, Prague: p. 324.

Chana, P. S. and Desai, S. B. 1992a. *Design of shear reinforcement against punching*. The Structural Engineer, 70(9): pp. 159–164.

Chana, P. S. and Desai, S. B. 1992b. *Membrane action, and design against punching shear*. The Structural Engineer, 70(19): pp. 339–343.

Einpaul J, Brantschen F, Fernández Ruiz M, and Muttoni A (2016) Performance of Punching Shear Reinforcement under Gravity Loading: Influence of Type and Detailing ACI Structural Journal, 113(4), pp. 827–838

Elghazouli, A. Y. and Izzuddin, B. A. 2004. *Realistic modelling of composite and reinforced concrete floor slabs under extreme loading. Part II: Verification and application*. Journal of Structural Engineering, 130(12): pp. 1985–1996.

Fernandez Ruiz, M. and Muttoni, A. 2009. *Applications of the critical shear crack theory to punching of reinforced concrete slabs with transverse reinforcement*. ACI Structural Journal, Vol. 106, No. 4: pp. 485-494.

Fernandez Ruiz, M., Mirzaei, Y. and Muttoni, A. 2013. *Post-punching behavior of flat slabs*. ACI Structural Journal, 110(5): pp.801–811.

fib. 2013. *fib Model Code for concrete structures 2010*. Fédération International du Béton, Lausanne, Switzerland.

Genikomsou A. 2015, *Nonlinear Finite Element Analysis of Punching Shear of Reinforced Concrete Slab Column Connections*, PhD thesis, University of Waterloo, Canada, pp. 257

Izzuddin, B. A. , Tao, X. Y. and Elghazouli, A.Y. 2004. *Realistic modeling of composite and reinforced concrete floor slabs under extreme loading*. *Part I: Analytical method*. Journal of Structural Engineering, 130(12): pp. 1972–1984.

Izzuddin, B. A. 1991. *Nonlinear dynamic analysis of framed Structures*. Thesis submitted for the degree of doctor of philosophy in the University of London, Department of Civil Engineering, Imperial College, London.

Keyvani, L., Sasani, M. & Mirzaei, Y., 2014. *Compressive membrane action in progressive collapse resistance of RC flat plates.* Engineering Structures, 59, pp.554–564.

Lips, S. 2012. *Punching of flat slabs with large amounts of shear reinforcement*. Thèse No 5409, École Polytechnique Fédérale de Lausanne.

Lips, S., Fernandez Ruiz, M. and Muttoni, A. 2012. *Experimental investigation on punching strength and deformation capacity of shear-reinforced slabs*. ACI Structural Journal, V. 109, No. 6: pp. 889-900.

Liu, J., Tian, Y., Orton, S. L. & Said, A. M., 2015a. *Resistance of Flat-Plate Buildings against Progressive Collapse*. *Part I : Modeling of Slab-Column Connections*. *Journal of Structural Engineering*, 141(12).

Liu, J., Tian, Y., Orton, S. L. & Said, A. M., 2015b. *Resistance of Flat-Plate Buildings against Progressive Collapse*. *Part II : System Response*. *Journal of Structural Engineering*, 141(12).

Menetrey, P. and Willam, K. J. 1995. *Triaxial failure criterion for concrete and its generalization*. ACI Structural Journal, 92(3): pp.311–318.

Muttoni, A. 2008. Punching shear strength of reinforced concrete slabs without transverse reinforcement. ACI Structural Journal, V. 105, No. 4: pp. 440-450.

Muttoni, A. and Schwartz, J. 1991. *Behaviour of beams and punching in slabs without shear reinforcement*. IABSE Colloquium, V. 62, Zurich, Switzerland: pp. 703-708.

Rizk, E., Marzouk, H. and Hussein, A. 2011. *Punching shear of thick plates with and without shear reinforcement*. ACI Structural Journal, 108(5): pp. 581-591.

Sagaseta, J., Muttoni, A., Ruiz, M. F. & Tassinari, L., 2011. *Non-axis-symmetrical punching shear around internal columns of RC slabs without transverse reinforcement.* Magazine of Concrete Research, 63(6), pp.441–457.

Setiawan, A., Vollum, R.L. and Macorini, L. 2019a. *Numerical and analytical investigation of internal slab-column connections subject to cyclic loading*. Engineering Structures, 184: pp. 535-554.

Setiawan, A., Vollum, R. L., Macorini, L. and Izzuddin, B. A. 2019b. *Efficient 3-D modelling of punching shear failure at slab-column connections by means of nonlinear joint elements.* Engineering Structures, 197: 109372.

Setiawan, A., Vollum, R. L., Macorini, L. and Izzuddin, B. A. 2020. *Punching shear design of RC flat slabs supported on wall corners.* Structural Concrete, https://doi.org/10.1002/suco.201900514.

Soares L. F. S. and Vollum, R. L. 2015. *Comparison of punching shear requirements in BS8110, EC2 and MC2010*. Magazine of Concrete Research, 67(24), pp.1315–1328.

Van Mier, J. G. M. 1986. *Multi-axial strain-softening of concrete, Part I: fracture, Part II: load-histories*. Materials and Structures, RILEM, 19: pp. 179-191.

Vecchio, F. J. and Collins, M. P. 1986. *The modified compression-field theory for reinforced concrete elements subjected to shear.* ACI Structural Journal, 83(2): pp. 219–231.

Vollum R.L, *Influences of shrinkage and construction loading on loss of tension stiffening in slabs*, Magazine of Concrete Research, 54, (2002), 273-282.

Vollum R.L., *Comparison of deflection calculations and span-to-depth ratios in BS 8110 and EC2*, Magazine of Concrete Research, 61, (2009), 465-476.

Table 1. Summary of material parameters and numerical input for NLFEA in ATENA.

No.	Parameter	Value/Reference
	Concrete constitutive model	
A1	Concrete elastic modulus	Model Code 2010
A2	Fracture energy	Model Code 2010
A3	Concrete tensile strength	Model Code 2010
A4	Smeared crack model	Fully-rotating crack
A5	Critical compressive displacement	0.5 mm
A6	Limit of compressive strength reduction due to cracking (MCFT)	$0.8f_c'$
A7	Eccentricity (defining the shape of the failure surface)	0.52
A8	Volume dilatation plastic factor	0
	Reinforcement bar model	
B1	Stress-strain relationship	Bilinear with minimal strain hardening
B2	Bond-slip model	Perfect bond
	Loading procedure and convergence criteria	
C1	Loading procedure	Static (force-controlled)
C2	Iteration method	Arc-length method
C3	Convergence criteria for displacement, residual, and absolute residual error	1%
C4	Convergence criteria for energy error	0.01%
	Mesh properties	
D1	Mesh size (finest)	25 x 25 x 25 mm^3
D2	Mesh element for concrete slab	8-noded hexahedral (linear)
D3	Mesh element for loading apparatus	4-noded tetrahedral (linear)
D4	Mesh element for flexural reinforcement bar	2-noded truss element (embedded)
D5	Mesh element for shear reinforcement bar	2-noded truss element (embedded)

Table 2. Summary of the predictions of the extended JSPM for slabs with shear reinforcement and ATENA 3-D solid model.

No	Category	Slab	Source	Measured / Predicted Punching Resistance	
				Extended JSPM	ATENA
1	Isolated	PL11	Lips et al. (2012)	1.018	0.858
2		PL12		1.042	0.910
3		PL7		1.022	0.911
4		2	Chana and Desai (1992a)	0.949	-
5		4		0.986	-
6		5		0.923	-
7		8		0.952	-
8		9		0.944	-
9	Continuous	FPS2	Chana and Desai (1992b)	0.898	-
10		FPS3		1.098	-
11		FPS4		1.120	-
12		FPS5		1.118	-
			Mean	1.006	0.893
			Standard deviation	0.073	0.025
			CoV	0.073	0.028